Monthly Notices
of the
ROYAL ASTRONOMICAL SOCIETY

MNRAS **471,** 1819–1829 (2017)
Advance Access publication 2017 July 6

doi:10.1093/mnras/stx1700

Chandra monitoring of the Galactic Centre magnetar SGR J1745−2900 during the initial 3.5 years of outburst decay

F. Coti Zelati,[1,2,3,4★] N. Rea,[2,4] R. Turolla,[5,6] J. A. Pons,[7] A. Papitto,[8] P. Esposito,[2] G. L. Israel,[8] S. Campana,[3] S. Zane,[6] A. Tiengo,[9,10,11] R. P. Mignani,[9,12] S. Mereghetti,[9] F. K. Baganoff,[13] D. Haggard,[14,15] G. Ponti,[16] D. F. Torres,[4,17] A. Borghese[2] and J. Elfritz[2]

[1]*Università dell'Insubria, via Valleggio 11, I-22100 Como, Italy*
[2]*Anton Pannekoek Institute for Astronomy, University of Amsterdam, Postbus 94249, NL-1090 GE Amsterdam, the Netherlands*
[3]*INAF – Osservatorio Astronomico di Brera, via Bianchi 46, I-23807 Merate (LC), Italy*
[4]*Institute of Space Sciences (ICE, CSIC–IEEC), Carrer de Can Magrans, S/N, E-08193 Barcelona, Spain*
[5]*Dipartimento di Fisica e Astronomia, Università di Padova, via F. Marzolo 8, I-35131 Padova, Italy*
[6]*Mullard Space Science Laboratory, University College London, Holmbury St. Mary, Dorking, Surrey RH5 6NT, UK*
[7]*Departament de Fisica Aplicada, Universitat d'Alacant, Ap. Correus 99, E-03080 Alacant, Spain*
[8]*INAF – Osservatorio Astronomico di Roma, via Frascati 33, I-00040 Monteporzio Catone, Roma, Italy*
[9]*INAF – Istituto di Astrofisica Spaziale e Fisica Cosmica, via E. Bassini 15, I-20133 Milano, Italy*
[10]*Istituto Universitario di Studi Superiori, Piazza della Vittoria 15, I-27100 Pavia, Italy*
[11]*Istituto Nazionale di Fisica Nucleare, Sezione di Pavia, via A. Bassi 6, I-27100 Pavia, Italy*
[12]*Kepler Institute of Astronomy, University of Zielona Góra, Lubuska 2, PL-65-265 Zielona Góra, Poland*
[13]*Kavli Institute for Astrophysics and Space Research, Massachusetts Institute of Technology, Cambridge, MA 02139, USA*
[14]*Department of Physics, McGill University, 3600 University St, Montreal, QC H3A 2T8, Canada*
[15]*McGill Space Institute, McGill University, Montreal, QC H3A 2A7, Canada*
[16]*Max Planck Institut für Extraterrestriche Physik, Giessenbachstrasse, D-85748 Garching, Germany*
[17]*Institució Catalana de Recerca i Estudis Avançats (ICREA), E-08010 Barcelona, Spain*

Accepted 2017 July 4. Received 2017 July 4; in original form 2017 April 26

ABSTRACT

We report on 3.5 yr of *Chandra* monitoring of the Galactic Centre magnetar SGR J1745−2900 since its outburst onset in 2013 April. The magnetar spin-down has shown at least two episodes of period derivative increases so far, and it has slowed down regularly in the past year or so. We observed a slightly increasing trend in the time evolution of the pulsed fraction, up to ∼55 per cent in the most recent observations. SGR J1745−2900 has not reached the quiescent level yet, and so far the overall outburst evolution can be interpreted in terms of a cooling hot region on the star surface. We discuss possible scenarios, showing in particular how the presence of a shrinking hotspot in this source is hardly reconcilable with internal crustal cooling and favours the untwisting bundle model for this outburst. Moreover, we also show how the emission from a single uniform hotspot is incompatible with the observed pulsed fraction evolution for any pair of viewing angles, suggesting an anisotropic emission pattern.

Key words: methods: data analysis – methods: observational – stars: magnetars – Galaxy: centre – X-rays: individual: SGR J1745−2900.

1 INTRODUCTION

One of the most enigmatic classes of the neutron star population comprises 23 objects whose observational manifestations can be explained only by exceptionally large magnetic fields, up to $\sim 10^{14}$–10^{15} G at the surface (see Olausen & Kaspi 2014 and the McGill Magnetar Catalog).[1] These neutron stars are commonly referred to as magnetars (see e.g. Thompson & Duncan 1993, 1995). In the past few years, new breakthroughs have clearly demonstrated how these strong fields might be hidden close or inside the neutron star crust (Rea et al. 2010; Tiengo et al. 2013; Turolla et al. 2011).

★ E-mail: francesco.cotizelati@brera.inaf.it

[1] http://www.physics.mcgill.ca/pulsar/magnetar/main.html

© 2017 The Authors
Published by Oxford University Press on behalf of the Royal Astronomical Society

Downloaded from https://academic.oup.com/mnras/article-abstract/471/2/1819/3930866/Chandra-monitoring-of-the-Galactic-Centre-magnetar
by Universidad de Alicante user
on 05 September 2017

Magnetars might release their large magnetic energy via steady X-ray emission ($L_X \sim 10^{32}$–10^{36} erg s^{-1}), or through bright flares and outbursts occurring at unpredictable times with significantly different time-scales (milliseconds to years) and energetics ($E \sim 10^{38}$–10^{45} erg; see Turolla, Zane & Watts 2015; Kaspi & Beloborodov 2017 for recent reviews). The continuous surveys of the hard X-ray/gamma-ray sky by the Burst Alert Telescope (Barthelmy et al. 2005) onboard *Swift* and the Gamma-ray Burst Monitor (Meegan et al. 2009) onboard *Fermi* represent nowadays one of the most fruitful channels to spot new members of the class, yielding a discovery rate of almost one candidate per year through the detection of their flaring activity.

SGR J1745−2900 is located at an angular distance of only 2.4 arcsec from the 4-million-solar mass black hole at the centre of the Milky Way, Sagittarius A* (Sgr A* hereafter). Its existence was heralded on 2013 April 25, following the detection of a ∼30-ms burst of soft gamma-rays (Kennea et al. 2013) and the discovery of a bright X-ray counterpart ($L_X \sim 5 \times 10^{35}$ erg s^{-1} for an assumed distance of 8.3 kpc; Genzel, Eisenhauer & Gillessen 2010). Coherent pulsations at a period of 3.76 s were detected both in the X-ray and radio bands (Kennea et al. 2013; Mori et al. 2013; Rea et al. 2013b; Shannon & Johnston 2013; Kaspi et al. 2014; Lynch et al. 2015; Pennucci et al. 2015), making SGR J1745−2900 the fourth confirmed radio-loud magnetar known to date after XTE J1810−197, 1E 1547−5408 and PSR 1622−4950 (Camilo et al. 2006, 2007; Levin et al. 2010).

SGR J1745−2900 has been regularly observed by *Chandra* and *XMM–Newton* since its discovery, as part of a monitoring program of the Galactic Centre primarily devoted to the investigation of the flaring activity of Sgr A* (e.g. Ponti et al. 2015 and references therein) and the effects of its interaction with the cold, dusty object G2. Analysis of the magnetar X-ray properties up to 2014 September unveiled an extremely slow decay of the X-ray flux (Coti Zelati et al. 2015), challenging the neutron star crustal cooling models successfully applied to other magnetar outburst decays. Although several observations have been performed with the European Photon Imaging Cameras (EPIC) on board *XMM–Newton* over the last 3 yr, SGR J1745−2900 was above the background level only during the first ∼1.5 yr of the outburst. This, and the presence of the nearby bright X-ray transient Swift J174540.7−290015 (discovered in 2016 February at only 16 arcsec from the magnetar and surrounded by a dust scattering halo; see Ponti et al. 2016), complicate detailed *XMM–Newton* studies of the outburst decay of SGR J1745−2900 at late times.[2] On the other hand, *Chandra* provides a prime opportunity to accurately investigate the evolution of the magnetar soft X-ray emission in the very long term, owing to the sub-arcsecond angular resolution of its X-ray instruments.

This paper presents 11 new *Chandra* observations of SGR J1745−2900 that, complemented with those we already described in our previous study (Coti Zelati et al. 2015), represent an unprecedented data set covering a time span of 3.5 yr since the outburst onset. We include the *XMM–Newton* data of the early phases of the outburst only to refine our timing solution, and refer to Coti Zelati et al. (2015) for details on the results of the spectral analysis. The paper is structured as follows. We describe the observations and the data reduction procedures in Section 2. We report on the timing and spectral analysis in Section 3. Discussion of our results follows in Section 4.

[2] The full width at half-maximum of the EPIC point spread function is about 6 arcsec.

2 OBSERVATIONS AND DATA EXTRACTION

The *Chandra X-ray Observatory* observed SGR J1745−2900 thirty-seven times between 2013 April 29 and 2016 October 14, for a total dead-time corrected on-source exposure time of about 1.17 Ms (see Table 1 for an updated journal of the observations). Except for the first pointing (ID 14701), which was carried out with the spectroscopic detector of the High Resolution Camera spectroscopic array (HRC-S; Zombeck et al. 1995), all observations were performed with the Advanced CCD Imaging Spectrometer spectroscopic array (ACIS-S; Garmire et al. 2003) operated in timed-exposure imaging mode and with faint telemetry format. A 1/8 subarray was adopted to achieve a time resolution of 0.44104 s and allow a proper characterization of the pulsations at the magnetar spin period, ∼3.76 s. The source was always positioned on the back-illuminated S3 chip.

The new data were processed and analysed using the *Chandra* Interactive Analysis of Observations software (CIAO, v. 4.8; Fruscione et al. 2006) and the most recent version of the calibration files (CALDB, v. 4.7.2). As it was done in our previous study (Coti Zelati et al. 2015), source photons were collected within a 1.5-arcsec circle centred on the source position. For each observation the background was estimated against many regions significantly differing in shape, size and proximity to the source. A 1.5-arcsec circle at the target position in archival (i.e. pre-outburst) ACIS-S observations of the field was also adopted to gauge the background level. All light curves were visually inspected and filtered for flares from particle-induced background (e.g. Markevitch et al. 2003). The source net count rate further decreased in the last 11 observations between 2014 October 20 and 2016 October 14 (see Table 1), and pile-up did not affect any of these data sets, as also confirmed by applying the PILEUP_MAP tool on the event files. All analyses were restricted to photons having energies between 0.3 and 8 keV. Photon arrival times were referred to the Solar system barycentre reference frame using the task AXBARY. Source and background spectra, redistribution matrices and ancillary response files were generated via SPECEXTRACT. Background-subtracted spectra were then grouped to have at least 50 counts in each energy channel, to enable the use of the χ^2 statistics to assess the goodness-of-fit. All uncertainties on the parameters are quoted at the 1σ confidence level for a single parameter of interest, unless otherwise specified.

SGR J1745−2900 was observed six more times between 2015 April 25 and 2016 July 24 with the ACIS imaging array (ACIS-I) onboard *Chandra*. In all these cases SGR J1745−2900 lied at an off-axis angle of about 9.8 arcmin from the aim point (the Sgr A* complex). The point spread function of the ACIS detectors is known to exhibit significant variations in size and shape across the focal plane, and at such off-axis angles the CIAO tool PSFSIZE_SRCS yields indeed an estimate of about 6 and 10 arcsec for the radii enclosing 50 and 90 per cent of the source photons, respectively (at an energy of 3 keV). Such large extraction regions encompass the X-ray counterpart of Sgr A*, and would certainly result in unreliable estimates of the magnetar flux. Moreover, the coarse time resolution achieved with the timed-exposure configuration of ACIS-I (Nyquist limit of about 6.48 s) precludes the detection of the pulsations. We hence decided not to include these observations in our analysis.

3 DATA ANALYSIS

3.1 Timing analysis

An updated timing solution was obtained by adopting the same procedure used to find Solution B reported by Coti Zelati et al.

Downloaded from https://academic.oup.com/mnras/article-abstract/471/2/1819/3930866/Chandra-monitoring-of-the-Galactic-Centre-magnetar
by Universidad de Alicante user
on 05 September 2017

Table 1. Journal of *Chandra* and *XMM–Newton*/EPIC observations of SGR J1745−2900. The 5-digit sequences refer to *Chandra* observations, the 10-digit sequences denote the *XMM–Newton* observations.

Obs. ID	Mid-point of observation (MJD)	Start time (TT) (yyyy-mm-dd hh:mm:ss)	End time (TT) (yyyy-mm-dd hh:mm:ss)	Exposure time (ks)	0.3–10 keV source net count rate (counts s^{-1})
14701[a]	56411.70	2013-04-29 15:14:12	2013-04-29 18:14:50	9.7	0.081 ± 0.003
14702	56424.55	2013-05-12 10:38:50	2013-05-12 15:35:56	13.7	0.545 ± 0.006
15040[b]	56437.63	2013-05-25 11:38:37	2013-05-25 18:50:50	23.8	0.150 ± 0.003
14703	56447.48	2013-06-04 08:45:16	2013-06-04 14:29:15	16.8	0.455 ± 0.005
15651[b]	56448.99	2013-06-05 21:32:38	2013-06-06 01:50:11	13.8	0.141 ± 0.003
15654[b]	56452.25	2013-06-09 04:26:16	2013-06-09 07:38:28	9.0	0.128 ± 0.004
14946	56475.41	2013-07-02 06:57:56	2013-07-02 12:46:18	18.2	0.392 ± 0.005
15041	56500.36	2013-07-27 01:27:17	2013-07-27 15:53:25	45.4	0.346 ± 0.003
15042	56516.25	2013-08-11 22:57:58	2013-08-12 13:07:47	45.7	0.317 ± 0.003
0724210201[c]	56535.19	2013-08-30 20:30:39	2013-08-31 12:28:26	55.6/57.2/57.2	0.657 ± 0.004
14945	56535.55	2013-08-31 10:12:46	2013-08-31 16:28:32	18.2	0.290 ± 0.004
0700980101[c]	56545.37	2013-09-10 03:18:13	2013-09-10 14:15:07	35.7/37.3/37.3	0.636 ± 0.005
15043	56549.30	2013-09-14 00:04:52	2013-09-14 14:19:20	45.4	0.275 ± 0.002
14944	56555.42	2013-09-20 07:02:56	2013-09-20 13:18:10	18.2	0.273 ± 0.004
0724210501[c]	56558.15	2013-09-22 21:33:13	2013-09-23 09:26:52	41.0/42.6/42.5	0.607 ± 0.005
15044	56570.01	2013-10-04 17:24:48	2013-10-05 07:01:03	42.7	0.255 ± 0.002
14943	56582.78	2013-10-17 15:41:05	2013-10-17 21:43:58	18.2	0.246 ± 0.004
14704	56588.62	2013-10-23 08:54:30	2013-10-23 20:43:44	36.3	0.240 ± 0.003
15045	56593.91	2013-10-28 14:31:14	2013-10-29 05:01:24	45.4	0.234 ± 0.002
16508	56709.77	2014-02-21 11:37:48	2014-02-22 01:25:55	43.4	0.156 ± 0.002
16211	56730.71	2014-03-14 10:18:27	2014-03-14 23:45:34	41.8	0.149 ± 0.002
0690441801[c]	56750.72	2014-04-03 05:23:24	2014-04-04 05:07:01	83.5/85.2/85.1	0.325 ± 0.003
16212	56751.40	2014-04-04 02:26:27	2014-04-04 16:49:26	45.4	0.135 ± 0.002
16213	56775.41	2014-04-28 02:45:05	2014-04-28 17:13:57	45.0	0.128 ± 0.002
16214	56797.31	2014-05-20 00:19:11	2014-05-20 14:49:18	45.4	0.118 ± 0.002
16210	56811.24	2014-06-03 02:59:23	2014-06-03 08:40:34	17.0	0.110 ± 0.003
16597	56842.98	2014-07-04 20:48:12	2014-07-05 02:21:32	16.5	0.097 ± 0.002
16215	56855.22	2014-07-16 22:43:52	2014-07-17 11:49:38	41.5	0.090 ± 0.001
16216	56871.43	2014-08-02 03:31:41	2014-08-02 17:09:53	42.7	0.085 ± 0.001
16217	56899.43	2014-08-30 04:50:12	2014-08-30 15:45:44	34.5	0.079 ± 0.002
0743630201[c]	56900.02	2014-08-30 19:37:28	2014-08-31 05:02:43	32.0/33.6/33.6	0.221 ± 0.004
0743630301[c]	56901.02	2014-08-31 20:40:57	2014-09-01 04:09:34	25.0/26.6/26.6	0.219 ± 0.004
0743630401[c]	56927.94	2014-09-27 17:47:50	2014-09-28 03:05:37	25.7/32.8/32.8	0.194 ± 0.004
0743630501[c]	56929.12	2014-09-28 21:19:11	2014-09-29 08:21:11	37.8/39.4/39.4	0.208 ± 0.004
16218[d]	56950.59	2014-10-20 08:22:28	2014-10-20 19:59:16	36.3	0.071 ± 0.001
16963[d]	57066.18	2015-02-13 00:42:04	2015-02-13 08:09:46	22.7	0.056 ± 0.002
16966[d]	57156.53	2015-05-14 08:46:51	2015-05-14 16:26:52	22.7	0.045 ± 0.001
16965[d]	57251.60	2015-08-17 10:35:47	2015-08-17 18:13:11	22.7	0.035 ± 0.001
16964[d]	57316.41	2015-10-21 06:04:57	2015-10-21 13:23:22	22.6	0.026 ± 0.001
18055[d]	57431.53	2016-02-13 08:59:23	2016-02-13 16:26:00	22.7	0.0133 ± 0.0008
18056[d]	57432.76	2016-02-14 14:46:01	2016-02-14 21:44:19	21.8	0.0146 ± 0.0009
18731[d]	57582.27	2016-07-12 18:23:59	2016-07-13 18:42:51	78.4	0.0112 ± 0.0004
18732[d]	57588.00	2016-07-18 12:01:38	2016-07-19 12:09:00	76.6	0.0118 ± 0.0004
18057[d]	57669.95	2016-10-08 19:07:12	2016-10-09 02:38:59	22.7	0.0123 ± 0.0008
18058[d]	57675.61	2016-10-14 10:47:43	2016-10-14 18:16:44	22.7	0.0122 ± 0.0007

Notes. [a] *Chandra*/HRC observation.
[b] *Chandra*/ACIS-S grating observations.
[c] *XMM–Newton* observations. Exposure times are reported for the pn, MOS1 and MOS2 cameras. Source net count rates refer to the pn detector.
[d] New unpublished *Chandra* observations.

(2015): we measured the spin frequency in each of the observations performed between 2014 February 21 (MJD 56709.5) and 2016 July 18 (MJD 56588.5) by fitting a linear function to the phases determined over 7-ks-long time intervals, and then fitted a quadratic function to the values of the spin frequency to determine the magnetar spin evolution. In the last two observations (in 2016 October), the counting statistics becomes so low to prevent the detection of the spin signal. A search for pulsations by means of a fast Fourier transform of the time series and the Z_n^2 test (Buccheri et al. 1983) with the number n of the assumed harmonics of the signal being varied from 1 to 3 did not reveal any peak above a confidence level of 3σ (estimated accounting for the number of independent frequencies examined and also for the number of harmonics in the case of the Z_n^2 test), either in the individual observations or in the merged event lists. The 3σ upper limit on the 0.3–8 keV pulsed fraction for any signal in the period range expected from extrapolation of the timing solution is about 45 per cent for both observations, accounting for the background level.

Fig. 1 shows the overall temporal evolution of the spin frequency from 2014 February to 2016 July, together with the best-fitting

Downloaded from https://academic.oup.com/mnras/article-abstract/471/2/1819/3930866/Chandra-monitoring-of-the-Galactic-Centre-magnetar
by Universidad de Alicante user
on 05 September 2017

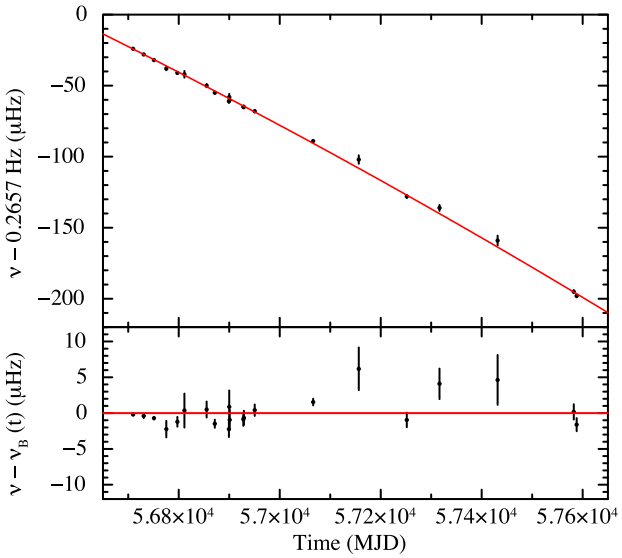

Figure 1. Top panel: temporal evolution of the spin frequency of SGR J1745−2900 over the time validity interval MJD 56709.5–57588.5 (see fig. 1 of Coti Zelati et al. 2015 for the temporal evolution at earlier times). The best-fitting model is marked by the red solid line (see Table 2). Bottom panel: residuals with respect to the model.

model and post-fit residuals. Table 2 reports the updated timing solution. The left-hand panel of Fig. 2 shows the 0.3–8 keV background-subtracted and exposure-corrected light curves folded on the best period, and sampled in 16 phase bins, for the first (ID 14702; top) and last (ID 18732; bottom) ACIS-S observations where the spin signal is detected. The right-hand panel displays the temporal evolution of the 0.3–8 keV pulsed fraction (PF) of SGR J1745−2900, derived either as PF = (max − min) × (max + min)$^{-1}$ (max and min refer to the maximum and the minimum of the pulse profile; see black data points in the figure) or by fitting a constant plus three sinusoidal functions to the pulse profiles, and dividing the value of the semi-amplitude measured for the fundamental sinusoidal component for the average count rate (the sinusoidal periods were fixed to those of the fundamental and harmonic components; see red data points in Fig. 2). SGR J1745−2900 shows a slightly increasing trend in the time evolution of its pulsed fraction, from an initial peak-to-peak value of about ∼37 per cent about 17–18 d after the outburst onset, up to ∼55 per cent after about 600 d.

3.2 Spectral analysis

All background-subtracted spectra were fitted within XSPEC[3] (version 12.9.0g; Arnaud 1996). We adopted the Tuebingen–Boulder model (TBABS in XSPEC), the abundances of Wilms, Allen & McCray (2000) and the cross-sections of Verner et al. (1996), to account for photoelectric absorption by neutral material in the interstellar medium (ISM) along the line of sight (LoS). The model developed by Davis (2001) was included for the first 12 data sets (obs IDs from 14702 to 15045, corresponding to the first ∼200 d of the outburst decay) to model the spectral distortions induced by pile-up (see Coti Zelati et al. 2015 for more details).

[3] http://heasarc.gsfc.nasa.gov/xanadu/xspec/

3.2.1 *Blackbody model*

We fitted all spectra together with an absorbed blackbody model. The hydrogen column density ($N_{\rm H}$) was tied up across all spectra, as no significant variations were observed over the whole 3.5 yr of monitoring, whereas the blackbody temperature and radius were left free to vary (this was indeed the best-fitting model describing the temporal evolution of the 0.3–8 keV spectral shape during the first 1.5 yr; Coti Zelati et al. 2015).

The joint fit yielded $\chi^2_\nu = 1.01$ for 2531 degrees of freedom (dof). The inferred column density is $N_{\rm H} = (1.87 \pm 0.01) \times 10^{23}$ cm^{-2}. Table 3 reports the best-fitting parameters for the blackbody component, and Fig. 3 shows the temporal evolution of the spectral parameters, the absorbed flux and the luminosity. The source is still fading, and the blackbody temperature still remains at a relatively high value of ∼0.65 keV about 1270 d after the outburst onset (to be compared with ∼0.9 keV about 2 weeks after the outburst peak). According to this model, the monotonic decline in the X-ray flux is then due mainly to the reduction of the blackbody radius, which decreased from an initial value of ∼2.5 down to ∼0.8 km (for an assumed distance of 8.3 kpc and as measured by an observer at infinity; see the left-hand panel of Fig. 5 for the spectra in the first and last ACIS-S observations). We gauged the rate of the hotspot shrinking by fitting an exponential function to the data points, and derived an e-folding time $\tau = 356^{+24}_{-22}$ d.

3.2.2 *Correction for dust scattering opacity*

Corrales et al. (2016) have recently noted that the absorption column density values measured towards heavily absorbed sources ($N_{\rm H} \gtrsim 10^{22}$ cm^{-2}) can be largely overestimated if the scattering of X-ray photons on interstellar dust grains is not taken into account properly in the spectral modelling (see also Smith, Valencic & Corrales 2016). The discrepancy is even more significant for small source extraction regions, because these barely account for the effect induced by dust scattering of removing photons from the LoS and spreading them into a surrounding halo.

The effects of the dust layer along the LoS towards the low-mass X-ray binary AX J1745.6−2901 (at only ∼1.46 arcmin from SGR J1745−2900) were recently investigated by Jin et al. (2017), who measured indeed a large alteration of the source spectral shape and flux for small extraction radii. The authors reported that the dust layer is likely located in the Galactic disc a few kpc away from AX J1745.6−2901, and thus might intervene also along the LoS towards SGR J1745−2900. As discussed by Ponti et al. (2017), this possibility is corroborated by radio observations of the pulsed emission from SGR J1745−2900, which led to constrain the position of the obscuring layer along the LoS of the magnetar at a distance of ∼5.8 kpc from the Galactic Centre within the spiral arms of the Milky Way (Bower et al. 2014).

As a further check, we hence decided to correct all magnetar spectra for dust scattering opacity by including in the spectral fits the FGCDUST model, developed by Jin et al. (2017) specifically for the case of AX J1745.6−2901 and applied by Ponti et al. (2017) on a sample of X-ray sources at the Galactic Centre. We derived $N_{\rm H} = (1.66 \pm 0.01) \times 10^{23}$ cm^{-2}, a value that is a factor of ∼13 per cent lower than that inferred when no correction is applied. Fig. 4 shows the variations introduced by this correction to the other spectral parameters. The effective temperature decreases from ∼0.8 to ∼0.6 keV and the emitting radius shrinks from ∼3.3 to ∼0.9 km (with e-folding time $\tau = 295^{+24}_{-21}$ d). The estimated X-ray luminosities are slightly larger compared to those derived without

Downloaded from https://academic.oup.com/mnras/article-abstract/471/2/1819/3930866/Chandra-monitoring-of-the-Galactic-Centre-magnetar
by Universidad de Alicante user
on 05 September 2017

Table 2. Timing solutions. The first solution (MJD 56411.6–56475.5) is taken from Rea et al. (2013b), the second (MJD 56500.1–56594.2) corresponds to Solution A by Coti Zelati et al. (2015) and the third is reported in Section 3.1 of this work and represents an updated solution of Solution B by Coti Zelati et al. (2015) over a longer temporal baseline. Uncertainties were evaluated at the 1σ confidence level, scaling the uncertainties by the value of the rms ($\sqrt{\chi^2_\nu}$) of the respective fit to account for the presence of unfitted residuals.

Validity range (MJD)	56411.6–56475.5	56500.1–56594.2	56709.5–57588.5
Epoch T_0 (MJD)	56424.5509871	56513.0	56710.0
$P(T_0)$ (s)	3.7635537(2)	3.76363799(7)	3.763982(3)
$\dot{P}(T_0)$ (s s^{-1})	$6.61(4) \times 10^{-12}$	$1.360(6) \times 10^{-11}$	$2.96(4) \times 10^{-11}$
$\ddot{P}$ (s s^{-2})	$4(3) \times 10^{-19}$	$3.7(2) \times 10^{-19}$	$0.67(20) \times 10^{-19}$
$\nu(T_0)$ (Hz)	0.265706368(14)	0.26570037(5)	0.2656761(2)
$\dot{\nu}(T_0)$ (Hz s^{-1})	$-4.67(3) \times 10^{-13}$	$-9.60(4) \times 10^{-13}$	$-2.09(3) \times 10^{-12}$
$\ddot{\nu}$ (Hz s^{-2})	$-3(2) \times 10^{-20}$	$-2.6(1) \times 10^{-20}$	$-0.47(11) \times 10^{-20}$
rms residual	0.15 s	0.396 s	3×10^{-5} s
χ^2_ν (dof)	0.85 (5)	6.14 (44)	3.16 (18)

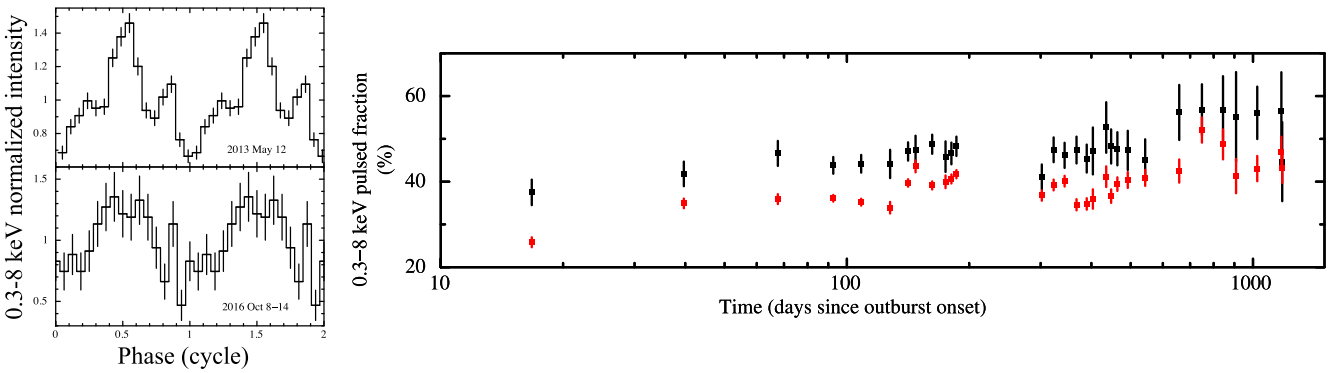

Figure 2. Left-hand panel: 0.3–8 keV background-subtracted and exposure-corrected light curves of SGR J1745−2900 folded on the best period for observation IDs 14702 and 18732, and sampled in 16 phase bins. For better visualization, the profiles have been phase aligned and two cycles are shown. Right-hand panel: temporal evolution of the 0.3–8 keV pulsed fraction. Black points refer to the peak-to-peak pulsed fraction, whereas red points refer to the values obtained from the modelling of the profiles (see text for details). Data points relative to the first 491 d of the outburst were already published by Coti Zelati et al. (2015).

correcting for the dust scattering halo, although we do not detect significant differences in the decay pattern. More sophisticated models are beyond the scope of the present work.

3.2.3 Depletion of elements in the ISM

We investigated the X-ray properties of the ISM along the LoS towards SGR J1745−2900 by substituting the TBABS model with the TBNEW model (Wilms et al. 2000), an improved version where the absorption column densities of different elements are allowed to vary in the fit. We repeated the joint fit leaving the abundances of all elements producing edges in the 1–8 keV energy range free to vary, and with and without the correction for the spectral distortions caused by the dust scattering halo. The abundances of most elements were found consistent with the solar values within the uncertainties, and were thus fixed to these values in the following analysis. The only exceptions are represented by iron and silicon. Adopting the elemental depletion factors of Wilms et al. (2000) for these elements, for which 30 and 10 per cent of the corresponding neutral atoms are expected to be in the gas phase, we computed 3σ upper limits well below the solar abundance values for both elements (see Table 4). These results are similar to those reported for the case of the close by X-ray transient Swift J174540.7−290015 (Ponti et al. 2016), and are suggestive of depletion of elements into dust grains in the ISM (see Jenkins 2009 for a review about depletion in the ISM).

3.3 Correlations, outburst energetics, quiescent properties

The extended monitoring campaign of SGR J1745−2900 allows us to search for possible correlations among different parameters across a wide range of values and spectral states. In the context of the blackbody model for the description of the continuum, we measure a significant correlation between the X-ray luminosity and the area of the thermal hotspot on the neutron star surface ($A_{\rm BB} = 4\pi R^2_{\rm BB}$, where $R_{\rm BB}$ is the blackbody radius inferred from the joint spectral fits; see Section 3.2.1). The correlation is significant at the 3.1σ level according to the Spearman rank test. To investigate the shape of the correlation, we fitted a power-law function of the form $L_{\rm X} = K(A_{\rm BB})^{\Gamma}$ to the data sets, and found the best-fitting parameters to be $\Gamma = 1.32 \pm 0.02$ and $K = (2.90 \pm 0.08) \times 10^{34}$ erg s^{-1} cm^{-2} ($\chi^2_\nu = 2.2$ for 31 dof). A completely consistent slope of $\Gamma = 1.33 \pm 0.02$ is obtained when all spectra are corrected for the dust scattering opacity along the LoS (see Section 3.2.2), although in this case we derived a lower normalization, $K = (1.90 \pm 0.06) \times 10^{34}$ erg s^{-1} cm^{-2} ($\chi^2_\nu = 3.8$ for 31 dof). The right-hand panel of Fig. 5 shows the 0.3–10 keV X-ray luminosity of SGR J1745−2900 as a function of the blackbody emitting area. The red solid line represents the best-fitting model, whereas the orange lines delimit the region on the L versus A plane within which data points should lie according to theoretical prediction of the untwisting bundle model for magnetar outbursts (see fig. 12 of Beloborodov & Li 2016). As discussed by Beloborodov & Li (2016), a broader range of allowed values on the

Downloaded from https://academic.oup.com/mnras/article-abstract/471/2/1819/3930866/Chandra-monitoring-of-the-Galactic-Centre-magnetar
by Universidad de Alicante user
on 05 September 2017

Table 3. *Chandra* spectral fitting results. Spectra of ACIS-S observations were fitted together with an absorbed blackbody model ($\chi^2_\nu = 1.01$ for 2506 dof). The derived absorption column density was $N_{\rm H} = (1.87 \pm 0.01) \times 10^{23}$ cm^{-2}. Spectra of the grating observations were fitted separately, as described by Coti Zelati et al. (2015). The blackbody radius and luminosity are evaluated for an observer at infinity and assuming a source distance of 8.3 kpc. Fluxes and luminosities are reported for the 0.3–10 keV energy interval.

Obs ID	$kT_{\rm BB}$ (keV)	$R_{\rm BB}$ (km)	Absorbed flux (10^{-12} erg cm^{-2} s^{-1})	Luminosity (10^{35} erg s^{-1})
14702	0.88 ± 0.01	$2.52^{+0.09}_{-0.08}$	$16.3^{+1.0}_{-0.8}$	4.9 ± 0.5
15040[a]	0.89 ± 0.02	2.5 ± 0.1	$15.5^{+0.03}_{-1.3}$	4.7 ± 0.5
14703	0.85 ± 0.01	$2.50^{+0.09}_{-0.08}$	$12.7^{+0.5}_{-0.6}$	4.1 ± 0.4
15651[a]	0.87 ± 0.03	2.4 ± 0.2	$12.5^{+0.07}_{-0.9}$	3.8 ± 0.4
15654[a]	0.88 ± 0.04	2.4 ± 0.2	$12.4^{+0.05}_{-0.9}$	3.5 ± 0.4
14946	0.83 ± 0.01	$2.39^{+0.09}_{-0.08}$	$10.4^{+0.4}_{-0.7}$	3.5 ± 0.3
15041	0.842 ± 0.008	$2.16^{+0.06}_{-0.05}$	$9.2^{+0.2}_{-0.3}$	$3.0^{+0.2}_{-0.4}$
15042	0.834 ± 0.008	2.09 ± 0.05	8.2 ± 0.3	$2.7^{+0.2}_{-0.4}$
14945	0.85 ± 0.01	$1.89^{+0.08}_{-0.07}$	$7.7^{+0.3}_{-0.4}$	2.4 ± 0.2
15043	0.824 ± 0.008	$2.03^{+0.06}_{-0.05}$	$7.2^{+0.2}_{-0.3}$	$2.4^{+0.2}_{-0.3}$
14944	0.84 ± 0.01	$1.88^{+0.08}_{-0.07}$	7.0 ± 0.4	$2.3^{+0.2}_{-0.3}$
15044	0.814 ± 0.009	1.98 ± 0.06	6.4 ± 0.2	$2.2^{+0.2}_{-0.3}$
14943	0.81 ± 0.01	$1.95^{+0.09}_{-0.08}$	$6.1^{+0.2}_{-0.4}$	2.1 ± 0.3
14704	0.810 ± 0.009	1.94 ± 0.06	$5.9^{+0.2}_{-0.3}$	2.1 ± 0.2
15045	0.825 ± 0.009	1.83 ± 0.05	$5.9^{+0.1}_{-0.2}$	$2.0^{+0.1}_{-0.2}$
16508	0.82 ± 0.01	1.49 ± 0.05	3.7 ± 0.1	$1.3^{+0.1}_{-0.2}$
16211	0.81 ± 0.01	1.50 ± 0.05	$3.4^{+0.1}_{-0.2}$	1.2 ± 0.2
16212	0.82 ± 0.01	1.38 ± 0.05	$3.1^{+0.1}_{-0.2}$	1.1 ± 0.1
16213	0.81 ± 0.01	1.37 ± 0.05	3.0 ± 0.1	1.0 ± 0.1
16214	0.81 ± 0.01	1.34 ± 0.05	2.7 ± 0.4	1.0 ± 0.1
16210	0.84 ± 0.02	$1.17^{+0.07}_{-0.06}$	$2.6^{+0.1}_{-0.3}$	0.9 ± 0.1
16597	0.77 ± 0.02	$1.36^{+0.09}_{-0.08}$	2.1 ± 0.4	0.8 ± 0.1
16215	0.81 ± 0.01	1.16 ± 0.05	2.1 ± 0.3	0.73 ± 0.08
16216	0.77 ± 0.01	$1.27^{+0.06}_{-0.05}$	1.9 ± 0.2	0.73 ± 0.07
16217	0.77 ± 0.01	1.24 ± 0.06	1.8 ± 0.2	0.69 ± 0.09
16218[b]	0.79 ± 0.01	$1.09^{+0.06}_{-0.05}$	1.7 ± 0.2	0.60 ± 0.07
16963[b]	0.79 ± 0.02	$0.98^{+0.07}_{-0.06}$	1.3 ± 0.3	0.46 ± 0.06
16966[b]	$0.76^{+0.03}_{-0.02}$	$0.97^{+0.09}_{-0.08}$	1.0 ± 0.2	0.40 ± 0.05
16965[b]	0.72 ± 0.02	$0.92^{+0.09}_{-0.07}$	0.7 ± 0.2	0.29 ± 0.04
16964[b]	0.74 ± 0.03	$0.79^{+0.10}_{-0.08}$	0.6 ± 0.2	0.24 ± 0.03
18055[b]	0.71 ± 0.04	$0.76^{+0.15}_{-0.11}$	0.4 ± 0.2	0.18 ± 0.03
18056[b]	$0.75^{+0.05}_{-0.04}$	$0.68^{+0.15}_{-0.12}$	0.4 ± 0.2	0.18 ± 0.02
18731[b]	0.70 ± 0.02	$0.70^{+0.07}_{-0.06}$	0.31 ± 0.02	0.15 ± 0.02
18732[b]	0.71 ± 0.02	$0.72^{+0.06}_{-0.05}$	0.35 ± 0.02	0.17 ± 0.02
18057[b]	0.66 ± 0.03	$0.79^{+0.12}_{-0.09}$	0.26 ± 0.02	0.14 ± 0.02
18058[b]	0.64 ± 0.03	$0.78^{+0.11}_{-0.10}$	0.23 ± 0.02	0.13 ± 0.02

Notes. [a] *Chandra*/ACIS-S grating observations.
[b] New unpublished observations.

L versus A plane may be attained depending on the value of the $B\phi\psi$ term (where B is the magnetic field strength at the surface, ϕ is the discharge voltage and ψ is the twist angle of the magnetosphere) and the possible variations of these parameters along the outburst decay.

The decay of the 0.3–10 keV luminosity can be satisfactorily reproduced by a phenomenological model consisting in a single exponential function plus a constant term: $L_{\rm X}(t) = A\exp(-t/\tau) + L_{\rm q}$ ($\chi^2_\nu = 0.81$ for 32 dof). Here t represents the time since the outburst onset (assumed to be coincident with the epoch of detection of the first soft gamma-ray burst from the source on 2013 April 25 at 19:15:25 UT; Kennea et al. 2013), τ is the e-folding time and $L_{\rm q}$ indicates the quiescent level (assumed to be $\lesssim 10^{34}$ erg s^{-1}, as derived from analysis of all archival *Chandra* observations of the Galactic Centre between 1999 and 2013 April). However, this model does not properly reproduce the very early phases of the outburst decay (within 40 d of the outburst onset; see the blue dashed line in the inset of Fig. 3), which are of paramount importance to adequately estimate the total energy released. A better modelling is obtained when adopting the superposition of two exponential functions: $L_{\rm X}(t) = \sum_{i=1}^{2} A_i \exp(-t/\tau_i) + L_{\rm q}$ (see the red solid line in Fig. 3). We obtained $\chi^2_\nu = 0.26$ for 30 dof, and determined $\tau_1 = 96^{+48}_{-39}$ d and $\tau_2 = 326^{+108}_{-43}$ d. Alternatively, a superexponential function of the form $L_{\rm X}(t) = B\exp[-(t/\tau)^\alpha] + L_{\rm q}$ provides a good description as well ($\chi^2_\nu = 0.24$ for 31 dof), yielding $\tau = 162^{+26}_{-28}$ d and $\alpha = 0.71 \pm 0.08$.

Extrapolation of the double-exponential model between the epoch of the outburst onset and that of the recovery of the quiescent state led to an estimate for the total energy released during the outburst of about 10^{43} erg in the 0.3–10 keV energy interval. A fully consistent value is estimated by adopting the superexponential function to model the luminosity evolution. This value should be considered only as a lower limit, owing to the unknown quiescent level of the source.

We then computed the outburst energetic with different assumptions on the true quiescent level of the source. Based on the values usually observed (and predicted) for magnetars undergoing major outbursts (Rea & Esposito 2011; Pons & Rea 2012; Li & Beloborodov 2015), we conservatively assume that the source attains a quiescent luminosity in the 10^{32}–10^{34} erg s^{-1} range, and consider in particular values of 10^{32}, 10^{33} and 10^{34} erg s^{-1} for the following estimates (see Table 5). Table 5 reports the outburst total energies and durations obtained always assuming the same double-exponential decay derived above. While the overall duration of the outburst significantly depends on the assumed quiescent flux (a factor of 2.5), the e-folding time and the total released energy have a much weaker dependence (only a factor of ∼1.3 and ∼1.1, respectively), and are in line with the values estimated for other magnetars.

We also estimated the upper limit on the temperature of SGR J1745−2900 detectable during quiescence by assuming that the X-ray thermal emission in this phase will arise from the whole neutron star surface, rather than from hotspots heated along the outburst. We then inferred the limiting value for the quiescent absorbed flux by assuming a blackbody spectral shape with $N_{\rm H} = 1.87 \times 10^{23}$ cm^{-2}, and the upper limit for the 0.3–8 keV count rate within the error circle of the source during pre-outburst ACIS-S observations performed between 2012 February 6 and 2012 October 31 (about 2.9 Ms in total), i.e. ∼0.001 counts s^{-1}. All values are reported in Table 5.

4 DISCUSSION

The extensive X-ray monitoring campaign of the Galactic Centre with *Chandra* allowed us to track the outburst evolution of magnetar SGR J1745−2900 over a time span of ∼3.5 yr since its onset, with an unprecedented detail. We measured an increase in the spin-down rate by a factor of ∼4.5 along 3 yr of outburst decay, from $\dot{P} \sim 6.6 \times 10^{-12}$ up to $\sim 3 \times 10^{-11}$ s s^{-1}. Changes in the rotational evolution of magnetars are commonly observed during outbursts. For example, 1E 1048.1−5937 displayed extreme variation in the spin-down rate after its outburst in 2011 December, with the frequency derivative first increasing nearly monotonically by a factor of ∼4.5–4.6, and then decaying back to the nominal spin-down value

Downloaded from https://academic.oup.com/mnras/article-abstract/471/2/1819/3930866/Chandra-monitoring-of-the-Galactic-Centre-magnetar
by Universidad de Alicante user
on 05 September 2017

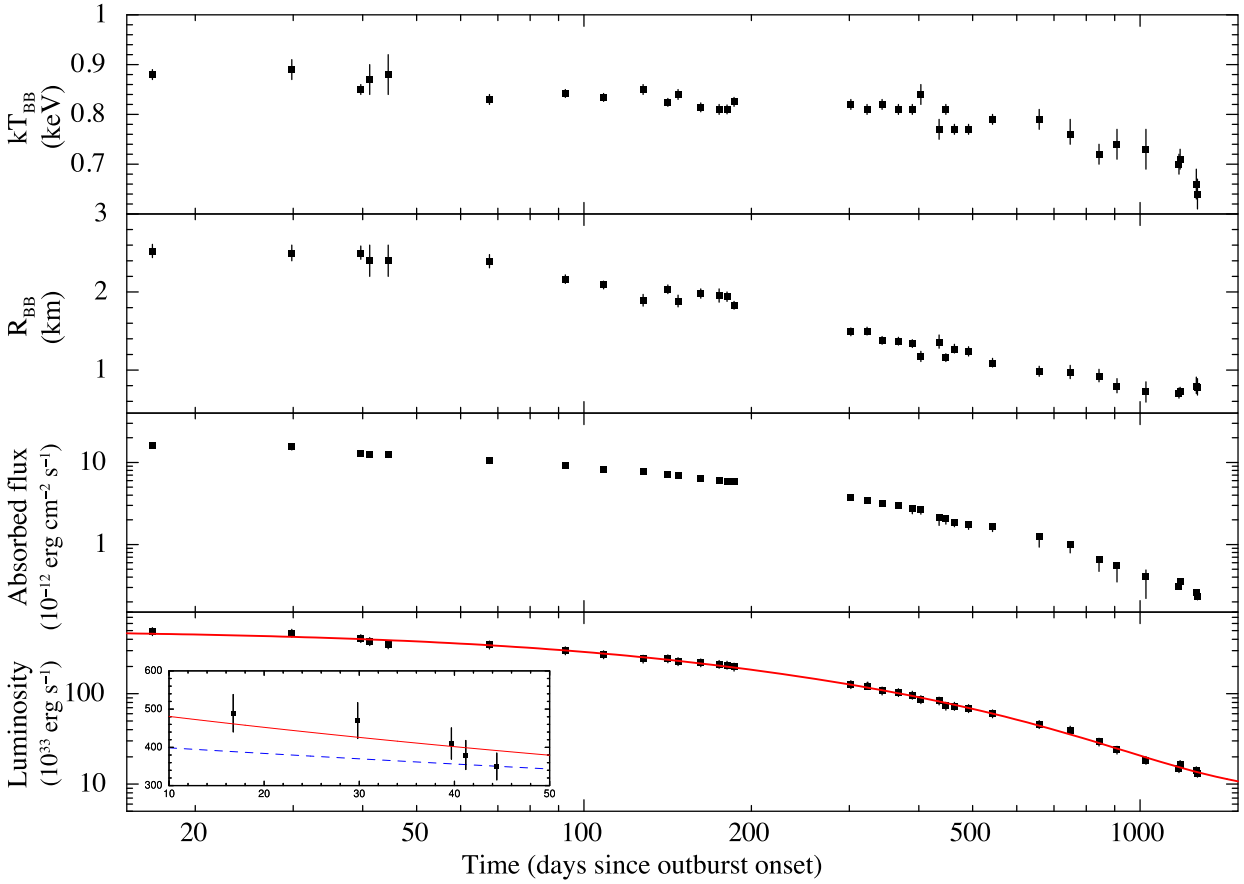

Figure 3. Time evolution of the blackbody temperature and radius, and of the 0.3–10 keV absorbed flux and luminosity of SGR J1745−2900. Spectra of the ACIS-S observations within the first ∼200 d of the outburst were corrected for the effects of pile-up. The best-fitting model for the luminosity decay (two exponential functions plus a constant) is marked by the red solid line in the bottom panel. The double exponential and the single exponential models are compared in the inset of the lower panel for the early stages of the outburst, and are depicted by the red solid line and the blue dashed line, respectively. Data points relative to the first 491 d of the outburst were already published by Coti Zelati et al. (2015).

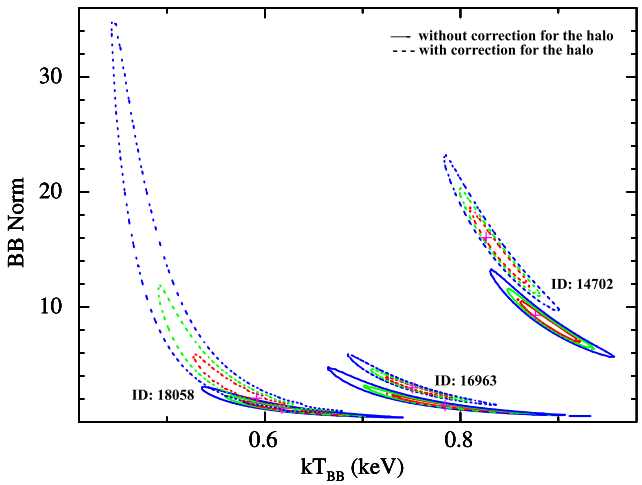

Figure 4. Contour plots in the *kT*–normalization plane for the best-fitting absorbed blackbody model applied to data sets acquired ∼17, 659 and 1268 d after the outburst onset (obs IDs 14702, 16963 and 18058, respectively). Contour plots derived without and with the correction for the effect of the dust scattering halo are denoted by solid and dashed lines, respectively. Red, green and blue refer to the 1σ, 2σ and 3σ confidence intervals, respectively.

in an oscillatory manner over a time-scale of months. Comparison with previous outbursts also suggested that a similar behaviour may repeat on a recurrence time of ∼1800 d (Archibald et al. 2015). SGR 1806−20 was also characterized by a significantly erratic behaviour in its timing properties after the giant flare in 2004 December, showing an increase by a factor of ∼2–3 in the long-term spin-down rate both in 2006 and 2008 (Younes, Kouveliotou & Kaspi 2015). Extended X-ray coverage of magnetar XTE J1810−197 between 2003 and 2014 led Camilo et al. (2016) and Pintore et al. (2016) to investigate the timing properties of the source over a long temporal baseline. The source was characterized by noisy spin-down up to 2007, with non-monotonic excursions in the frequency derivative by a factor of $\gtrsim 8$, and was then observed to spin-down regularly in the following 7 yr.

The evolution of the timing properties of SGR J1745−2900 could be compatible with the predictions of the untwisting bundle model for magnetar outbursts (Beloborodov 2009). According to this scenario, the evolution of magnetar outbursts is regulated by the presence of a twisted bundle of current-carrying closed field lines in a confined region of the magnetosphere. As the twist grows during the early stages of the outburst, a larger fraction of closed field lines open out across the light cylinder, yielding an increase of the dipolar magnetic field at the light cylinder radius and hence of the spin-down torque acting on the star (see also Parfrey, Beloborodov & Hui 2013). For a moderate initial twist ($\psi_0 < 1$ rad),

Downloaded from https://academic.oup.com/mnras/article-abstract/471/2/1819/3930866/Chandra-monitoring-of-the-Galactic-Centre-magnetar
by Universidad de Alicante user
on 05 September 2017

Table 4. Hydrogen absorption column densities and 3σ upper limits on the abundances of iron (Fe) and silicon (Si) in the ISM along the LoS towards SGR J1745−2900. The upper limits were derived from the joint spectral fits of the ACIS-S observations.

Model	$N_{\rm H}$ (10^{23} cm^{-2})	$A_{\rm Fe}$ ($A_{\rm Z,\odot}$)	$A_{\rm Si}$ ($A_{\rm Z,\odot}$)
TBNEW*BBODYRAD	$2.30^{+0.01}_{-0.04}$	<0.20	<0.42
FGCDUST*TBNEW*BBODYRAD	$2.04^{+0.01}_{-0.02}$	<0.19	<0.36

the process leading to the enhancement in the spin-down rate might lag with respect to the epoch of the outburst onset, with a delay comparable to the time required for the twist amplitude to grow from its initial value up to $\psi \sim 1$ rad. Conversely, if the initial twist is strong ($\psi_0 \gtrsim 1$ rad), this mechanism should operate soon after the twist is implanted (Beloborodov 2009). In the former regime, the variation in the spin-down rate can be related to the twist amplitude as

$$2\pi \frac{\Delta \dot{P}}{\dot{P}} \sim \psi^2 \ln \frac{u_*}{u_{\rm LC}}, \quad (1)$$

where u is the area of the bundle calculated at the star surface (u_*) and at the light cylinder radius ($u_{\rm LC}$). For a strong initial twist, this simple estimate does not hold anymore, and must be substituted by a full non-linear computation.

The overall fractional increase in the spin-down torque of SGR J1745−2900, $\Delta \dot{P}/\dot{P} \sim 4.5$, appears incompatible with the presence of a moderate twist, according to the formula above. It might be instead the result of prolonged, delayed effects of a strong growing twist during the initial phases of the outburst. However, detailed calculations would be needed to explore this possibility. The spin-down torque is expected to decrease back to that of the dipole field as the twist gradually decays in the subsequent phases of the outburst. A reversal in the rotational evolution should hence be observed at some point in future observations according to this model. The case of SGR J1745−2900 may be indeed similar to that of XTE J1810−197, where a decreasing trend in the spin-down rate was detected only after the first $\gtrsim$ 500 d of the outburst (Camilo et al. 2016; Pintore et al. 2016). The ongoing *Chandra* monitoring program of the Galactic Centre will allow us to explore this possibility in SGR J1745−2900. Alternatively, the observed torque changes might be ascribed either to the occurrence of (at least two) glitches that the sparse observations could not resolve properly in the timing residuals, or to an increase of the particle density in the magnetosphere possibly related to the outburst activity.

The pulsed fraction showed a slightly increasing trend in time, from an initial peak-to-peak value of ≈40 per cent during the very early stages of the outburst, up to ≈55 per cent about 3 yr later (see Fig. 2). A similar behaviour has been observed so far only in the low-field magnetar SGR 0418+5729, which reached values for the pulsed fraction of ∼70–80 per cent at the quiescent level (see fig. 1 by Rea et al. 2013a).

All spectra can be successfully described by a blackbody model, corrected by the large absorption by the neutral material in the ISM along the LoS towards the source ($N_{\rm H} \sim 1.7 \times 10^{23}$ cm^{-2}, comparable with that estimated for other sources located at the Galactic Centre, including Sgr A*, using the same abundances and cross-sections; see Ponti et al. 2017). The effects of dust scattering in the ISM were also taken into account, yielding only subtle variations in the values of the spectral parameters modelling the continuum emission and of the luminosities.

SGR J1745−2900 is still recovering from the outburst episode that led to its discovery in 2013 April. The spectral evolution implied by the blackbody model suggests the presence of a hotspot on the neutron star surface, presumably formed during the episode that led to the outburst activation, and then progressively shrinking and cooling. However, some care must be exercised in extracting physical information from the modelling of the thermal emission with a simple blackbody spectrum, in particular in assessing the shrinking of the emitting region. The true emission process responsible for the thermal radiation from magnetars is still largely unknown. It may be related to the presence of an atmosphere, albeit with properties quite different from those of standard atmospheres around passively cooling neutron stars, or even arise from a condensed surface: in both cases the spectrum is expected to be thermal but not necessarily blackbody-like (see e.g. Potekhin 2014 for a recent review). The fitting with more physically motivated models might return somehow different values of the area and temperature of the emitting region, possibly showing a different trend for the hotspot radius. We have also fitted all the spectral data sets using the Nobili–Turolla–Zane (NTZ) model (Nobili, Turolla & Zane 2008a, Nobili, Turolla & Zane2008b), which is a three-dimensional implementation of the resonant cyclotron up-scattering of thermal photons coming from the entire star surface (assumed to be at the same temperature) on to electrons flowing in a globally twisted magnetosphere of a magnetar. We obtained an equally statistically acceptable result ($\chi^2_\nu = 0.99$ for 2467 dof) by leaving all parameters free to vary, although no tight constraints could be derived on the values of the bulk motion velocity of the magnetospheric charged particles and the twist angle (as expected given the thermal spectral shape). The estimated absorption column density, $N_{\rm H} = (1.98 \pm 0.02) \times 10^{23}$ cm^{-2}, is slightly larger compared to that derived from the blackbody model, whereas the effective temperature, fluxes and luminosities turn out to be fully consistent with the blackbody values within the uncertainties. These results indicate that the overall magnetar spectral evolution along the outburst decay can be properly described also without necessarily invoking the existence of a shrinking emission region on the neutron star surface.

Taking the blackbody model as a baseline, the observed properties can be hardly reconciled with crustal cooling models, for which the

Table 5. Estimates on the quiescent properties of SGR J1745−2900. The outburst duration is estimated by considering the epoch at which the source attains the quiescent level within an uncertainty of 10 per cent on the value for the quiescent luminosity, according to the double-exponential model. τ_1 and τ_2 represent the e-folding times of the exponential functions, E refers to the estimated energy released, $kT_{\rm q}$ and $F_{\rm X,q}$ are the upper limits on the blackbody temperature and flux detectable in quiescence, respectively. The radius of the blackbody emitting region was fixed to 10 km.

Assumed $L_{\rm X,q}$ (erg s^{-1})	Outburst duration (d)	τ_1 ()	τ_2 (d)	E (erg)	$kT_{\rm q}$ (keV)	$F_{\rm X,q}$ (erg cm^{-2} s^{-1})	χ^2_ν (dof)
1×10^{32}	∼5300	157^{+29}_{-26}	550^{+131}_{-65}	1.1×10^{43}	0.05	5×10^{-15}	0.31 (31)
1×10^{33}	∼3800	152^{+30}_{-27}	518^{+115}_{-57}	1.1×10^{43}	0.09	7×10^{-15}	0.31 (31)
1×10^{34}	∼1700	74^{+33}_{-28}	290^{+16}_{-13}	9.5×10^{42}	0.17	1×10^{-14}	0.27 (31)

Downloaded from https://academic.oup.com/mnras/article-abstract/471/2/1819/3930866/Chandra-monitoring-of-the-Galactic-Centre-magnetar
by Universidad de Alicante user
on 05 September 2017

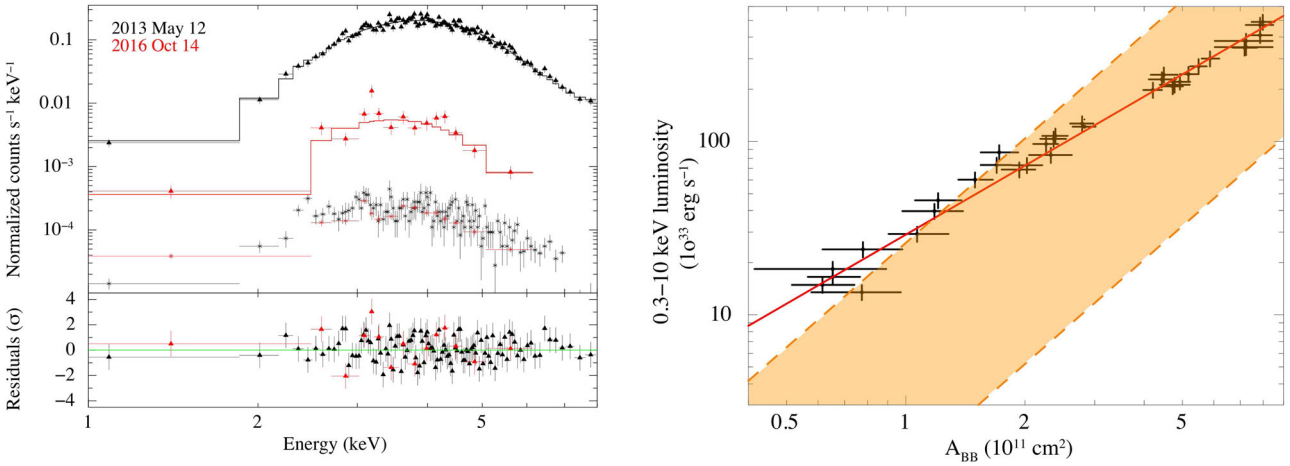

Figure 5. Left-hand panel: background-subtracted spectra of SGR J1745−2900 corresponding to the first (black data points; ID: 14702) and last (red data points; ID: 18058) *Chandra* ACIS-S observations. Background spectra, rescaled to the area of the source extraction region, are also shown. For plotting purpose, spectra are shown in the 1–8 keV after rebinning the data points. The solid lines represent the best-fitting absorbed blackbody model (see the text for details). Post-fit residuals in units of standard deviations are plotted at the bottom. Right-hand panel: X-ray luminosity of SGR J1745−2900 as a function of the blackbody area. The red solid line denotes the fit with a power-law function, the orange dashed lines delimit the region where data points should be located according to the model of Beloborodov (2009; see also Beloborodov & Li 2016).

size of the emitting region is expected to remain fairly constant while the temperature decreases as part of the internal heat is conducted up to the outer layers of the crust (see Coti Zelati et al. 2015 for our previous simulations). On the other hand, the observed behaviour is again a natural prediction of the untwisting bundle model. Recent studies have shown that the resistive untwisting of magnetic bundles in magnetar outbursts might last a few years (e.g. Beloborodov & Li 2016). The prolonged, sustained emission of SGR J1745−2900 may be indeed due to the continuous bombardment of returning currents on to the neutron star surface. The gradual dissipation of the twist should lead to the reduction of both the size and temperature of the region at the base of the bundle as the rate of charged particles impacting upon the surface decreases. This is in broad agreement with the shrinking of the hotspot derived by spectral fits (see Fig. 5).[4]

Fig. 6 shows the contour plots of the magnetar pulsed fraction as a function of the viewing angles χ and ξ (i.e. the inclination of the LoS and the spot normal with respect to the rotation axis, respectively) at different epochs of the outburst decay. For our computations we adopted the analytical expressions derived by Turolla & Nobili (2013), which account for the effects of gravitational light-bending, and we assumed isotropic blackbody emission from a finite, uniform, circular cap on the neutron star surface. We set the blackbody temperature and radius equal to the measured values at the corresponding epochs, and took into account the uncertainties on both parameters (see Table 3). We then calculated the values of χ and ξ in such a way that the corresponding pulsed fractions were compatible with the observed values within the uncertainties (see the right-hand panel of Fig. 2). No favourable viewing geometry exists that is able to reproduce the observed variations of the pulsed fraction between the two epochs. This is suggestive of an anisotropic emission pattern from the spot, or a change in its position on the surface in time or even a more complex shape of the emitting region with respect to that of a simple circular cap as assumed in our code. However, the latter possibility appears less likely, because modelling the emission with an elongated spot or multiple spots would predict an even smaller pulsed fraction, at odds with the large values observed in the data.

The observations carried out in the past 2 yr have confirmed the extremely slow luminosity decay on which we have already reported in our previous study concerning the first year and a half of outburst decay (Coti Zelati et al. 2015). The decay is more rapid in the first 100 d of the outburst (e-folding time $\tau_1 \sim 96$ d) than in the following stages ($\tau_2 \sim 330$ d). Prolonged outburst decays have been observed also in other magnetars. For example, SGR 1627−41 underwent an outburst in 1998, and several observations with different X-ray instruments revealed that the source returned to its quiescent level in about 10 yr (Esposito et al. 2008). Scholz, Kaspi & Cumming (2014) reported on X-ray observations of Swift J1822.3−1606 over the first ∼2 yr of the outburst evolution, and showed that the flux decay could be phenomenologically described in terms of multiple exponential functions with high decay time-scales (up to about 320 d for a triple-exponential model). More recently, Younes et al. (2015) observed for SGR 1806−20 an exponential decay of the flux between 2003 and 2011, with a characteristic time-scale of ∼1.5 yr.

For SGR J1745−2900 we set a lower limit (owing to the yet unknown quiescent level of the source) on the total energy released in the outburst of $\gtrsim 10^{43}$ erg. Estimates for the outburst energetic, duration and maximum blackbody temperature detectable during quiescence were also derived under different assumptions for the quiescent level. In particular, according to our estimates, SGR J1745−2900 may reach its pre-outburst level either soon at the end of 2017 or on a much longer time-scale of about 10 yr, depending on the source quiescent luminosity (either 1×10^{34} or 1×10^{32} erg s^{-1}, respectively). The exquisite spatial resolution of the instruments onboard *Chandra* provides us with the unique opportunity to study the magnetar properties down to its faintest flux levels, and the ongoing monitoring campaign will allow us to put more stringent constraints on the source quiescent

[4] A power-law-like tail associated with resonant cyclotron scattering of thermal photons on to the charged particles in the magnetic twist might be observed in the spectra along the overall decay. For the specific case of SGR J1745−2900, a faint power-law component was only detected above ∼8 keV, thanks to the broader energy coverage and the larger effective area of the instruments onboard *XMM–Newton* (see Coti Zelati et al. 2015) and *NuSTAR* (see Kaspi et al. 2014).

Downloaded from https://academic.oup.com/mnras/article-abstract/471/2/1819/3930866/Chandra-monitoring-of-the-Galactic-Centre-magnetar
by Universidad de Alicante user
on 05 September 2017

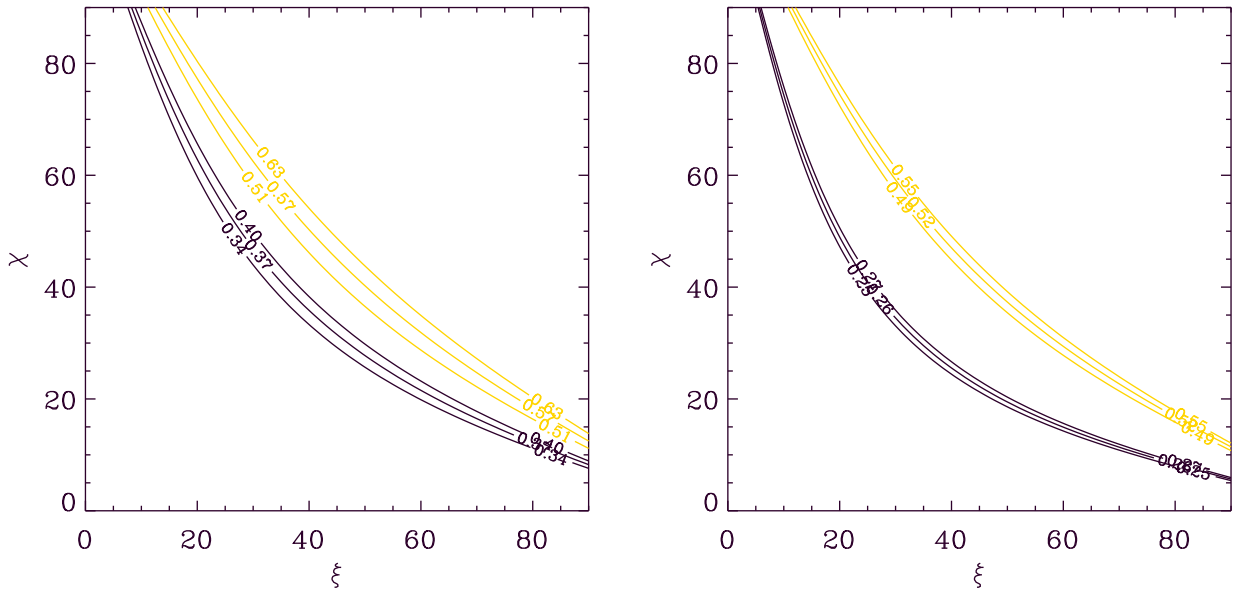

Figure 6. Contour plots for the pulsed fraction, plotted as a function of the viewing angles, for observations performed ∼17 d (ID 14702; black lines) and ∼750 d (ID 16966; yellow lines) after the outburst onset (see the text for details). 1σ confidence intervals are reported. The contours in the left-hand panel refer to the peak-to-peak pulsed fractions, whereas those in the right-hand panel refer to the pulsed fractions obtained from the modelling of the pulse profiles (see the text for details).

properties and hence on the energy and time-scales involved in the outburst.

ACKNOWLEDGEMENTS

The scientific results reported in this paper are based on observations obtained with the *Chandra X-ray Observatory* and *XMM–Newton*, an ESA science mission with instruments and contributions directly funded by ESA Member States and the National Aeronautics and Space Administration (NASA). This research has made extensive use of software provided by the *Chandra* X-ray Center [CXC, operated for and on behalf of NASA by the Smithsonian Astrophysical Observatory (SAO) under contract NAS8–03060] in the application package CIAO, and of softwares and tools provided by the High Energy Astrophysics Science Archive Research Center (HEASARC), which is a service of the Astrophysics Science Division at NASA/GSFC and the High Energy Astrophysics Division of the Smithsonian Astrophysical Observatory. FCZ, NR, PE, AB and JE acknowledge funding in the framework of a Vidi award A.2320.0076 of the Netherlands Organisation for Scientific Research (PI: N. Rea), and the European COST Action MP1304 (NewCOMPSTAR). FCZ, NR and DFT are supported by grant AYA2015-71042-P. NR and DFT are also supported by grant SGR2014-1073. RT, AT and SM acknowledge financial contribution from the agreement ASI/INAF I/037/12/0 and from PRIN INAF 2014. JAP acknowledges support by grants AYA2015-66899-C2-2-P and PROMETEOII-2014-069. AP is supported via an EU Marie Sködowska-Curie Individual fellowship under contract no. 660657-TMSP-H2020-MSCA-IF-2014. RPM acknowledges financial support from an 'Occhialini Fellowship'. DH acknowledges support from a Natural Sciences and Engineering Research Council of Canada Discovery Grant and a Fonds de recherche du Québec Nature et Technologies Nouveaux Chercheurs Grant. GP acknowledges support via the Bundesministerium für Wirtschaft und Technologie/Deutsches Zentrum für Luft-und Raumfahrt (BMWI/DLR, FKZ 50 OR 1604) and the Max Planck Society. FCZ acknowledges Chichuan Jin for providing the *Chandra* ACIS-S version of the dust scattering model. We thank Giovanni Fazio, Joseph Hora, Gordon Garmire and Steven Willner for sharing their data and the referee for helpful comments.

REFERENCES

Archibald R. F., Kaspi V. M., Ng C.-Y., Scholz P., Beardmore A. P., Gehrels N., Kennea J. A., 2015, ApJ, 800, 33
Arnaud K. A., 1996, in Jacoby G. H., Barnes J., eds, ASP Conf. Ser. Vol. 101, Astronomical Data Analysis Software and Systems V. Astron. Soc. Pac., San Francisco, p. 17
Barthelmy S. D. et al., 2005, Space Sci. Rev., 120, 143
Beloborodov A. M., 2009, ApJ, 703, 1044
Beloborodov A. M., Li X., 2016, ApJ, 833, 261
Bower G. et al., 2014, ApJ, 780, L2
Buccheri R. et al., 1983, A&A, 128, 245
Camilo F., Ransom S. M., Halpern J. P., Reynolds J., Helfand D. J., Zimmerman N., Sarkissian J., 2006, Nature, 442, 892
Camilo F., Ransom S. M., Halpern J. P., Reynolds J., 2007, ApJ, 666, L93
Camilo F. et al., 2016, ApJ, 820, 110
Corrales L. R., Garcia J., Wilms J., Baganoff F., 2016, MNRAS, 458, 1345
Coti Zelati F. et al., 2015, MNRAS, 449, 2685
Davis J. E., 2001, ApJ, 562, 575
Esposito P. et al., 2008, MNRAS, 390, L34
Fruscione A. et al., 2006, in Silva D. R., Doxsey R. E., eds, Proc. SPIE, Vol. 6270, Observatory Operations: Strategies, Processes, and Systems. SPIE, Bellingham, p. 62701V
Garmire G. P., Bautz M. W., Ford P. G., Nousek J. A., Ricker G. R., Jr, 2003, in Truemper J. E., Tananbaum H. D., eds, Proc. SPIE, Vol. 4851, X-Ray and Gamma-Ray Telescopes and Instruments for Astronomy. SPIE, Bellingham, p. 28
Genzel R., Eisenhauer F., Gillessen S., 2010, Rev. Modern Phys., 82, 3121
Jenkins E. B., 2009, ApJ, 700, 1299
Jin C., Ponti G., Haberl F., Smith R., 2017, MNRAS, 468, 2532
Kaspi V. M., Beloborodov A. M., 2017, ARA&A, in press, preprint (arXiv:1703.00068)

Downloaded from https://academic.oup.com/mnras/article-abstract/471/2/1819/3930866/Chandra-monitoring-of-the-Galactic-Centre-magnetar
by Universidad de Alicante user
on 05 September 2017

Kaspi V. M. et al., 2014, ApJ, 786, 84
Kennea J. A. et al., 2013, ApJ, 770, L24
Levin L. et al., 2010, ApJ, 721, L33
Li X., Beloborodov A. M., 2015, ApJ, 815, 25
Lynch R. S., Archibald R. F., Kaspi V. M., Scholz P., 2015, ApJ, 806, 266
Markevitch M. et al., 2003, ApJ, 583, 70
Meegan C. et al., 2009, ApJ, 702, 791
Mori K. et al., 2013, ApJ, 770, L23
Nobili L., Turolla R., Zane S., 2008a, MNRAS, 386, 1527
Nobili L., Turolla R., Zane S., 2008b, MNRAS, 389, 989
Olausen S. A., Kaspi V. M., 2014, ApJS, 212, 6
Parfrey K., Beloborodov A. M., Hui L., 2013, ApJ, 774, 92
Pennucci T. T. et al., 2015, ApJ, 808, 81
Pintore F. et al., 2016, MNRAS, 458, 2088
Pons J. A., Rea N., 2012, ApJ, 750, L6
Ponti G. et al., 2015, MNRAS, 454, 1525
Ponti G. et al., 2016, MNRAS, 461, 2688
Ponti G. et al., 2017, MNRAS, 468, 2447
Potekhin A. Y., 2014, Phys. Uspekhi, 57, 735
Rea N., Esposito P., 2011, in Torres D. F., Rea N., eds, Astrophysics and Space Science Proceedings, High-Energy Emission from Pulsars and Their Systems. Springer-Verlag, Berlin, p. 247
Rea N. et al., 2010, Science, 330, 944
Rea N. et al., 2013a, ApJ, 770, 65
Rea N. et al., 2013b, ApJ, 775, L34
Scholz P., Kaspi V. M., Cumming A., 2014, ApJ, 786, 62
Shannon R. M., Johnston S., 2013, MNRAS, 435, 29
Smith R. K., Valencic L. A., Corrales L., 2016, ApJ, 818, 143
Thompson C., Duncan R. C., 1993, ApJ, 408, 194
Thompson C., Duncan R. C., 1995, MNRAS, 275, 255
Tiengo A. et al., 2013, Nature, 500, 312
Turolla R., Nobili L., 2013, ApJ, 768, 147
Turolla R., Zane S., Pons J. A., Esposito P., Rea N., 2011, ApJ, 740, 105
Turolla R., Zane S., Watts A., 2015, Rep. Progress Phys., 78, 116901
Verner D. A., Ferland G. J., Korista K. T., Yakovlev D. G., 1996, ApJ, 465, 487
Wilms J., Allen A., McCray R., 2000, ApJ, 542, 914
Younes G., Kouveliotou C., Kaspi V. M., 2015, ApJ, 809, 165
Zombeck M. V., Chappell J. H., Kenter A. T., Moore R. W., Murray S. S., Fraser G. W., Serio S., 1995, Proc. SPIE, 2518, 96

This paper has been typeset from a TEX/LATEX file prepared by the author.

Downloaded from https://academic.oup.com/mnras/article-abstract/471/2/1819/3930866/Chandra-monitoring-of-the-Galactic-Centre-magnetar
by Universidad de Alicante user
on 05 September 2017